Research, Society and Development, v. 9, n. 11, e92191110433, 2020
(CC BY 4.0) | ISSN 2525-3409 | DOI: http://dx.Doi.org/10.33448/rsd-v9i11.10433

Computational simulation of nanostructured lipid carrier containing lipids from Cupuassu (*Theobroma grandiflorum)* seed fat: Design, interaction and molecular dynamic study

Simulação computacional do carreador lipídico nanoestruturado contendo lipídeos da gordura da semente do Cupuaçu (*Theobroma grandiflorum):* Desenho, interação e estudo de dinâmica molecular

Simulacíon por computadora del portador lipídico nanoestructurado que contiene lípidos de la grasa de la semilla de Cupuaçú (*Theobroma grandiflorum):* Diseño, interacción y studio de dinámica molecular

Received: 11/19/2020 | Reviewed: 11/30/2020 | Accept: 12/04/2020 | Published: 12/07/2020

Ana Paula Bastos Ferreira Vieira
ORCID: https://orcid.org/0000-0001-8936-7420
Federal University of Pará, Brazil
E-mail: anabastos02@gmail.com
Natália de Farias Silva
ORCID: https://orcid.org/0000-0001-5105-4090
Federal University of Pará, Brazil
E-mail: natyflavonas@yahoo.com.br
Davi do Socorro Barros Brasil
ORCID: https://orcid.org/0000-0002-1461-7306
Federal University of Pará, Brazil
E-mail: dsbbrasil18@gmail.com
José Otávio Carréra Silva Júnior
ORCID: https://orcid.org/0000-0003-1691-1039
Federal University of Pará, Brazil
E-mail: carrera@ufpa.br
Roseane Maria Ribeiro Costa
ORCID: https://orcid.org/0000-0001-5470-0617
Federal University of Pará, Brazil
E-mail: roseaneribeiro01@yahoo.com.br

Abstract

Drug delivery systems are constantly evolving and developing, as well as the search for promising and effective formulations for drug delivery. Computational simulation methods enable the development of complex systems, such as nanostructured lipid carriers (NLC), the understanding of interaction and dynamics between drug molecule and its transporter. In this work, aimed to simulate a NLC containing cupuassu fat triacylglycerols, carnauba wax and caprylic/capric acid triacylglycerol, stabilized with Tween 80 and Pluronic and ketoconazole enantiomer as drug was simulated. Initially, lipid mixtures were studied by Differential Scanning Calorimetry and X-ray diffraction. Subsequently, computational studies were carried out, among which Molecular Docking of ketoconazole to the lipid mixture and Molecular Dynamics of NLC system containing ketoconazole. From the results obtained it was possible to observe the main binding affinities of the drug and provide a better NLC formulation. It was also possible to propose a three-dimensional NLC model that was stable after molecular dynamics and ideal for future experimental studies.

Keywords: Computational simulation; Nanostructured lipid carrier; Cupuassu.

Resumo

Os sistemas de liberação controlada de fármacos estão em constante evolução e desenvolvimento, assim como a busca de formulações promissoras e eficazes para a entrega de drogas. Métodos de simulação computacional viabilizam o desenvolvimento de sistemas complexos, como os carreadores lipídicos nanoestruturados (NLC), a compreensão da interação e da dinâmica entre a molécula de fármaco e o seu transportador. Neste estudo objetivou-se simular um NLC contendo triacilgliceróis da gordura de cupuaçu, a cera de carnaúba e o triacilglicerol de ácido cáprico/caprílico, estabilizados com tween 80 e pluronic e com um enantiômero do cetoconazol como fármaco. Inicialmente, misturas lipídicas foram estudadas por métodos de Calorimetria Exploratória Diferencial e Difração de Raios-X. Posteriormente, foram realizados estudos computacionais, dentre os quais, tem-se a docagem molecular do cetoconazol à mistura lipídica e a Dinâmica Molecular de um sistema NLC contendo o cetoconazol. A partir dos resultados obtidos foi possível observar as principais afinidades de ligação do fármaco e propiciar uma melhor formulação de NLC com o fármaco. Também foi possível propor um modelo tridimensional de NLC que se mostrou estável após dinâmica molecular e ideal para futuros estudos experimentais.

Palavras-chave: Simulação computacional; Carreador lipídico nanoestruturado; Cupuaçu.

Resumen

Los sistemas de administración de fármacos controlados están en constante evolución y desarrollo, al igual que la búsqueda de formulaciones prometedoras y eficaces para la administración de fármacos. Los métodos de simulación por computadora permiten el desarrollo de sistemas complejos, como los portadores de lípidos de la nanoestructura (NLC), la comprensión de la interacción y la dinámica entre la molécula del fármaco y su portador. El objetivo de este estudio fue simular un NLC que contiene triacilgliceroles de grasa de cupuaçú, cera de carnauba y triacilglicerol de ácido cáprico/caprílico, estabilizado con tween 80 y pluronic y con un enantiómero de ketoconazol como fármaco. Inicialmente, las mezclas de lípidos se estudiaron mediante métodos de la calorimetría diferencial de barrido y difracción de rayos X. Posteriormente, se realizaron estudios computacionales, entre los que se encuentra el acoplamiento molecular del ketoconazol a la mezcla lipídica y la Dinámica Molecular de un sistema NLC que contiene ketoconazol. A partir de los resultados obtenidos fue posible observar las principales afinidades de unión del fármaco y aportar una mejor formulación de NLC con el fármaco. También fue posible proponer un modelo tridimensional de NLC que resultó ser estable después de la dinámica molecular e ideal para futuros estudios experimentales.

Palabras clave: Simulación por computadora; Portador lipídico nanoestructurado; Cupuaçú.

1. Introduction

The search for new drug delivery systems (DDS) is boosted by the possibility of obtaining pharmaceutical forms with higher drug bioavailability, specific targeting, prolonged effect, controlled and constant release, low toxicity and good biodegradability, as well as being versatile and adaptable to various drugs (Puri, et al., 2009; Ramezani & Shamsara, 2016). However, time and cost involved in the preliminary experimental tests are inconvenient factors for the preparation of formulations. In this way, Molecular Modeling and Computational Simulation have been highlighted as powerful tools for drug design. Computational models allow targeting promising formulations, anticipate molecular and biological properties, decrease the amount of test compositions, facilitate screening for formulation experimental design and optimize those that have already been developed but presented limitations (Carvalho, et al., 2003; Ramezanpour, et al., 2016; Sant'Anna, 2009).

Currently, computational methods are used to study DDS properties, such as self-assembly of components, physical-chemical characteristics, circulation, DDS's performance

in targets and membrane-cell and intracellular interaction. As well as estimating DDS behavior in various environmental conditions, such as pH, temperature, solutes concentration, external magnetic fields, interactions with other biomolecules and other variables that may affect their efficiency and yield (Ramezanpour, et al., 2016). Different types of DDS have already been studied by computer simulation, such as dendrimers (Zhang, et al., 2014), polymer-based (Ramezani & Shamsara, 2016), peptide and nucleic acid base (Todorova, et al., 2014), carbon nanotubes based (Lai & Barnard, 2015), gold nanoparticles and the lipid based (Brancolini, et al., 2012).

Interest in lipid-based DDS, such as liposomes (Jämbeck, et al., 2014), micelles (Lee & Pastor, 2011) and lipid nanoparticles (Galindo, et al., 2020; Rosa, et al., 2020; Santos, et al., 2012), is increasing not only because of their ability to encapsulate and transport drugs and biomolecules but also because of the versatility of compositions that can be generated (Ramezanpour, et al., 2016). Nanostructured Lipid Carriers (NLC) are an evolution of lipid nanoparticles and represent an alternative system with solid and liquid lipids composing the lipid matrix, with greater storage capacity and stability, and release of the encapsulated drugs (Haider, et al., 2020; Salvi & Pawar, 2019). Several types of lipids can compose the lipid matrix, but depending on the chemical affinity for the drug, they may directly influence the success of DDS. Lipids of natural origin stand out mainly for modern medicine, as they have additional properties and are sources of bioactive compounds with multiple health benefits (Lacatusu et al., 2014), such as fat extracted from Cupuassu (*Theobroma grandiflorum*) seeds, with a strong tendency towards topical application due to the possibility of obtaining phytonutrients as a balanced composition of saturated and unsaturated fatty acids, predominantly of oleic acid and stearic acid, amino acids, vitamins (A, C, B1, B2 and B3) and important flavonoids (catechin, epicatechin, quercetin, kaempferol and theograndins (I and II) (Costa, et al., 2020; Quast, et al., 2011).

In this work, a nanostructured lipid carrier was proposed using Cupuassu fat triacylglycerols, carnauba wax and caprylic/capric acid triacylglycerol (TAC) integrating the lipid matrix, Tween 80 and Pluronic as surfactants and a ketoconazole enantiomer as a drug model representative. Computational simulations were performed for NLC in order to elucidate the three-dimensional structures, study molecular and electrostatic properties, as well as intermolecular interactions between drug and carrier. Results of this study can be used as support for guiding future development of NLC formulations, anticipating experimental tests and helping to obtain thriving formulations.

2. Methodology

This is a semi-empirical study of quantitative and descriptive character (Pereira, et al., 2018), which use in silico and experimentals approaches. Therefore, this study was subdivided in experimental section and computational section.

2.1 Experimental section

Characterization and Selection of Lipid Mixtures: Three lipid mixtures (coded as M01, M02 and M03) were initially developed with ratios following the fat/wax 2:1 and the amount of Capric/Caprylic acid triacylglycerol was proportional to 100% of the mixture. M01 with proportion of 40% Cupuassu fat and 20% carnauba wax; For M02, 30% Cupuassu fat and 15% carnauba wax; and for M03 20% Cupuassu fat and 10% carnauba wax. Selection of lipid mixture was performed from the experimental results of Differential Scanning Calorimetry (DSC) and X-ray Diffraction (XRD) from isolated samples and mixtures.

For DSC analysis samples were heated to 100°C/15 minutes, and then cooled to room temperature for recrystallization (Souto, et al., 2006). Hermetically sealed aluminum crucible, temperature up to 200 ° C, heating rate of 10 ° C / min, inert nitrogen atmosphere (N_2) and flow rate of 50mL / min were used. Differential scanning calorimetry performed in Shimadzu® DSC-60 Plus (Kyoto, Japan). Data obtained were treated in Shimadzu® TA-60WS software (Kyoto, Japan). XRD analysis was performed by D8 Advance diffractometer, Bruker® (Ettlingen, Germany), with Cu tube, Cu radiation (Kα = 1.540598 Å), angular range (2Θ) of 10-80, tube voltage 40kV , 40 mA tube current, 0.6 mm diverging slit, 2.5 ° soller slit, and Ni kβ filter. Diffractogram was collected with an angular pitch of 0.02 ° and time per step 1s.

2.2 Computational section

2.2.1 Structural Models

Initially major structures of NLC constituents were established to be used as representative. Three-dimensional (3D) structures were initially treated separately, some were obtained from NCBI (National Center for Biotechnology Information), and others were generated using ChemDraw Ultra 12 software (CambridgeSoft Corporation, Cambridge, MA)

and subsequently the 3D structure was obtained with Chem3D 12 program (CambridgeSoft Corporation, Cambridge, MA). Followed by optimization using DTF method with functional B3LYP hybrid and basis set 6-31G (d, p) established in Gaussian 09 (Plumley & Dannenberg, 2011).

2.2.2 Molecular Electrostatic Potential (MEP)

The Molecular Electrostatic Potential (MEP) was applied to study molecular reactivity patterns. This is a highly informative tool for electronic charges distribution of a molecule of interest. Here, MEP surfaces were derived from DTF method with hybrid functional B3LYP and basis set 6-31G (d, p) (Plumley & Dannenberg, 2011) calculated and generated in Spartan Student 8 software (wavefunction, Inc.) (Engel & Reid, 2006). These surfaces correspond to an isodensity value of 0.05 a.u.

2.2.3 Lipid Matrix Simulation

To simulate a three-dimensional matrix, number of molecules used, corresponded to the percentage of the selected lipid mixture component, as described in the Table 1. Lipid matrix was simulated in Packmol Software Package (Martínez et al., 2009) with simple mixture model and 70Å orthorhombic box. Three-dimensional image was generated in Visual Molecular Dynamycs (VMD) program (Xu, et al., 1996).

Table 1. Number of molecules for the components of the lipid mixture relative to their proportion (%).

Components	M01		M02		M03	
	%	Nm	%	Nm	%	Nm
SOO	40	16	30	12	20	8
SOS		11		8		5
CER	20	30	15	23	10	15
TAC	40	97	55	133	70	169

Nm: Number of molecules/ SOO and SOS: Cupuassu fat triacylglycerols/ CER: Carnauba wax/ TAC: Capric/Caprylic acid triacylglycerols. Source: Authors.

In Table 1, shows the proportion of the mixtures M01, M02 and M03 for each component, cupuassu Fat Triacylglycerols (SOO and SOS), carnauba Wax and

Capric/Caprylic acid triacylglycerols, where the number of molecules corresponds to the percentage of each component the mixtures.

2.2.4 Molecular Docking

Molecular Docking study was performed with AutoDock 4.2 software (Morris, et al., 2009) for the selected lipid mixture with regular precision with a maximum of 100 conformations per candidate. Kollman charges required for calculation were added and non-polar hydrogens suppressed. Rotatable bonds of the ligand (ketoconazole) were automatically defined (Silva, et al., 2017; Silva, et al., 2020). Conformations were classified using scoring function and Lamarckian genetic algorithm. After locating possible binding sites, conformations of the doped complex were optimized using the steepest decent algorithm until convergence, with a maximum of 20 interactions. The grid box dimensions were (X = 22 / Y = 14 / Z = 14).

2.2.5 Molecular Dynamics Simulation

The proposal of 10% lipids, 1% surfactants, 1% drug and 88% water (Souto, 2013) was used for NLC simulation, taking into account the number of molecules related to the following components (Table 2).

Table 2. Number of molecules for the components of the NLC relative to their proportion.

Components	Proportion (%)	Number of molecules
SOS	10	4
SOO		3
CER		7
TAC		85
PLU	0,5	18
T80	0,5	5
CET	1	11
WATER	88	29416

SOO and SOS: Cupuassu fat triacylglycerols / CER: Carnauba wax / TAC: Capric/Caprylic acid triacylglycerols/ T80: tween 80/ PLU: pluronic/ CET: Ketoconazole. Source**:** Authors.

In Table 2, shows the percentage experimental values were converted into number of molecules related to the following components: Cupuassu fat triacylglycerols, carnauba wax,

caprylic/capric acid triacylglycerols, tween 80, pluronic, ketoconazole and water, so that these could be used for computational simulation.

Files of automated Topology Builder (ATB) topologies were generated for system constituents which were later minimized and thermalized to 298K. Coordinates of each atom of the system remained fixed during thermalization, with a constant force of 1.0 x 103 $KJ.mol^{-1}nm^{-2}$. Aqueous systems were solvated with water molecules through the simple point charge model: Simple Point Charge (SPC/TIP3). Verlet-Verlet algorithm and canonical ensemble (Namba, et al., 2008) were used. The long-range electrostatic contributions were treated through Reaction Field. Yet electrostatic and van der Waals interactions used to treat the short-range interactions occur within a cut-off radius of 1.4 nm, avoiding the occurrence of interactions between atoms and their own virtual images three-dimensionally replicated by periodic boundary conditions. Simulation was performed in 20ns, using FF99S parameter set within the Gromacs program (Van Der Spoel, et al., 2005).

3. Results and Discussion

3.1 Lipid matrix selection

Best DSC and XRD results were established as a criterion to select the lipid matrix. DSC curves are demonstrated in Figure 1 and in addition, Table 3 shows data concerning melting temperature, on-set temperature and enthalpy.

Figure 1. DSC curves of the (a) Cupuassu Fat and Carnauba wax, (b) of the mixtures.

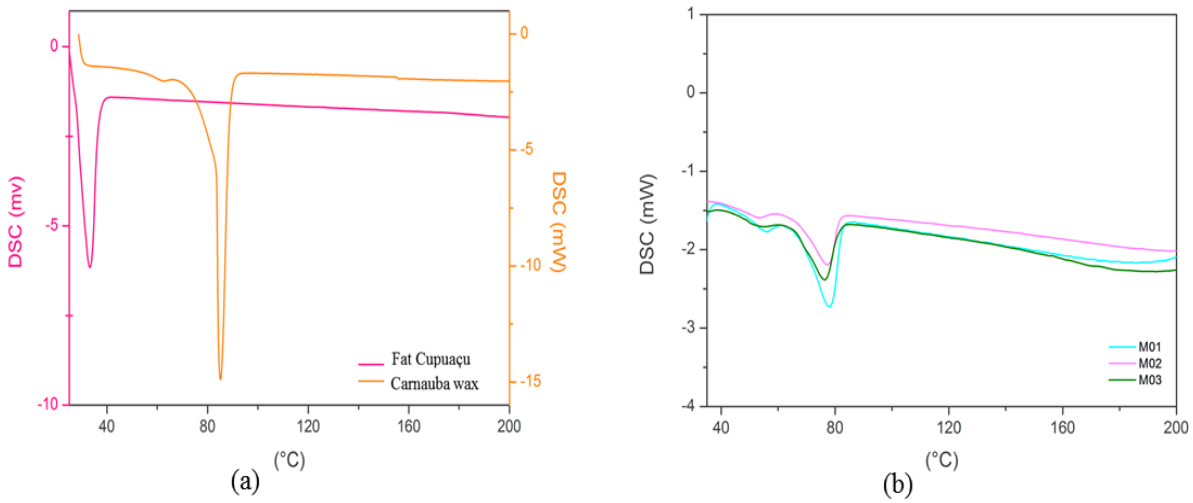

Source: Authors.

In Figure 1, shows the DSC curves the mixtures lipids (M01, M02 and M03), Cupuassu fat and carnauba wax. Each peak observed in the curves, representing a thermal event that occurred by the temperature variation.

Table 3. Melting temperature, On-set temperature and enthalpy of the isolated components and mixtures.

Components	Melting (°C)	On-set (°C)	Enthalpy (J/g)
M01	78,06	68,45	-21,74
M02	77,25	66,78	-17,75
M03	76,31	65,39	-15,17
CF*	33,14	27,89	-72,25
CW*	85,12	83,38	-174,01

* FC: Cupuassu fat; CW: Carnauba Wax. Source**:** Authors.

In Table 3, shows temperature values of the beginning of the thermal event (on-set), the moment of fusion (melting) and the heat enthalpy generated for each component.

An endothermic event was observed in the Figure 1a, DSC curve of carnauba wax, at 85.12°C related to its melting point, with on-set extrapolation of 83.38°C and enthalpy of -174.01 J/g; the carnauba wax melting occurs between 80 and 86°C (Milanovic, et al., 2010). DSC curve of Cupuassu fat, demonstrated in Figure 1a, presented an endothermic event related to its melting point at 33.14°C with onset of 27.89°C and enthalpy of -72.2 J/g; its fusion occurs between 30 to 38°C (Gilabert-Escrivá, et al., 2002). Endothermic events of the mixtures were observed in the Figure 1, with melting occurring between 76-78°C; in DSC curves a decrease in height and widening of peaks was observed. All mixtures showed smaller enthalpy variations than the components evaluated separately, as observed in the Figure 1b, indicating that there had been interaction between the components, as well as formation of new crystalline structures. Interaction between solid and liquid lipids in the lipid matrix may alter melting temperature and enthalpy, generating a less ordered crystalline structure. This effect has already been evidenced by other authors (Yang, et al., 2014). Among mixtures, M02 and M03 presented lower values of enthalpy and melting temperature, indicating that they may form crystalline structures of less order.

XRD curves are demonstrated in Figure 2. In the Figure 2a, the X-ray diffractogram of the fat shows a long intensity peak at 19.46° and several other peaks of short spacing and medium intensity at 10.77°, 22.25°, 22.84°, 23.76° and 24.33°, which are in agreement with

values found by other authors (Quast, et al., 2011; Silva et al., 2009). In the Figure 2b the Carnauba wax presented two high intensity peaks, one at 21.51° and another at 23.82°, characteristic of this wax (Villalobos-Hernández & Müller-Goymann, 2006). One can clearly see changes in peak intensity in the diffractogram of the mixtures (according the Figure 2c). Mixture M01 presented two peaks of medium intensity at 19.51º and 23.86º and one of high intensity at 21.56º. In mixture M02 two peaks of medium intensity were also observed at 19.45º and 23.97º and one of low intensity at 21.56º. In mixture M03 there is a peak broadening at 22º followed by a peak of medium intensity at 21.54º and a decrease at 23.97º. Among the three mixtures, M03 presented lower intensity peaks, suggesting structures with lower crystallinity.

Figure 2. XRD of the (a) Cupuassu fat, (b) Carnauba wax, (c) mixtures.

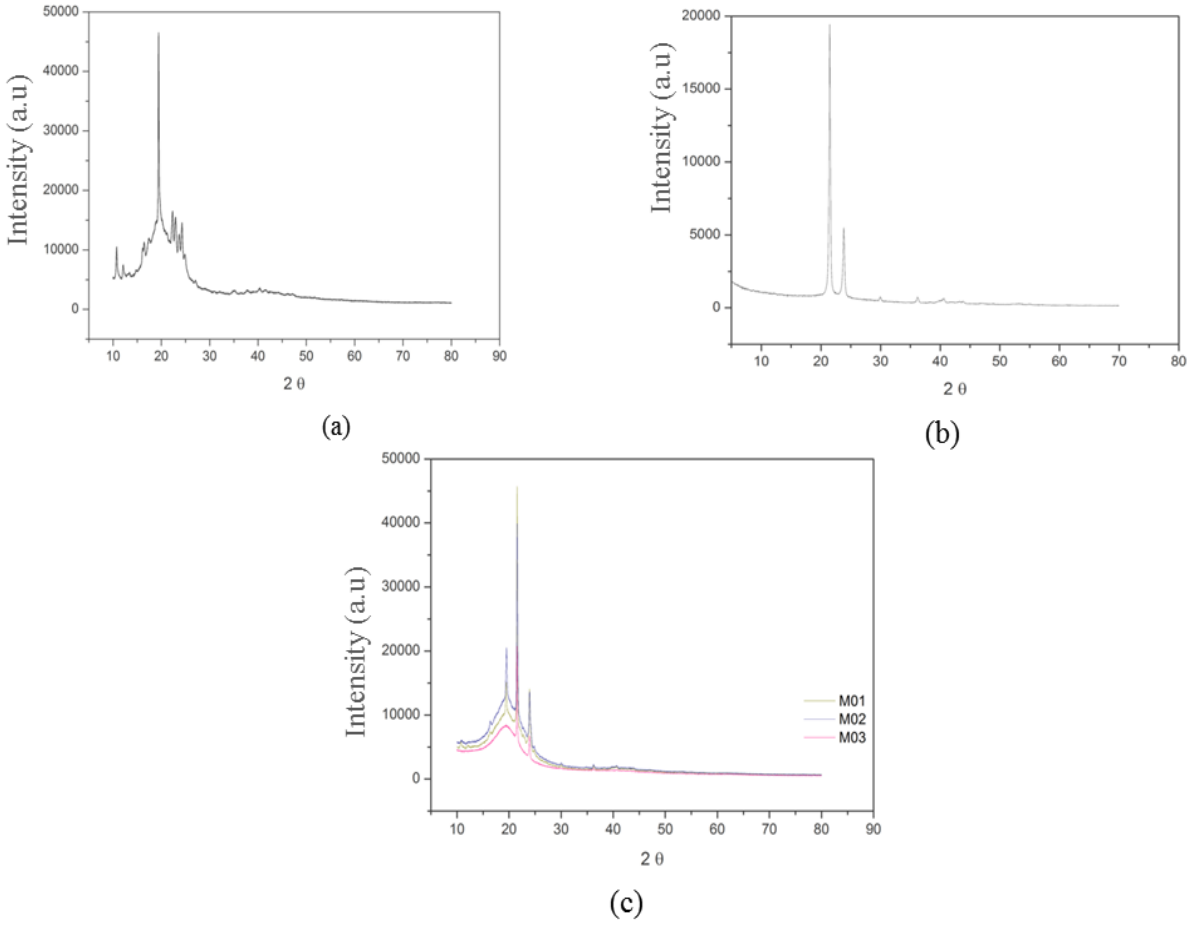

Source: Authors.

Observed in Figure 2, that the intensity of each peak generated samples studies. This is due to the fact the samples have varied structures crystallinity. Some tend to be more

crystalline and others more amorphize, this directly refletct the spacing and intensity peak in the diffractograms the Figure 2.

Changes observed in diffractograms when comparing fat, wax and mixtures may indicate that there has been a polymorphic change of the lipid mixtures in order to decrease crystalline arrangement and there was a greater tendency to amorphize, especially in mixture M03. Relating DSC results to those of XRD one can say that M03 is the mixture of greater interest to produce NLC, once the crystalline form of the lipid matrix directly influences drug release profile, as in general, very ordered lipid- solid matrices have a lower diffusion rate of active substance, and amorphous regions facilitate drug incorporation.

3.2 Obtaining the three-dimensional structures models

Initially, structures representing NLC components were established, as observed in the Figure 3 and Figure 4. In Cupuassu fat the predominant constituents are triglycerides, where SOS (1,3-distearoyl-2-oleoylglycerol), as the Figure 3a shows, corresponds to approximately 30% and SOO (1-stearoyl-2,3-dioleoylglycerol) to 20% (Figure 3b), together accounting for about 50% of the composition (Gilabert-Escrivá, et al., 2002; Quast, et al., 2011), so they were set as major and representative of Cupuassu fat. In the Figure 3c we have the Carnauba wax, a simple ester composed of myricyl cerotate (Silva, et al., 2017). Capric/Caprylic acid triacylglycerol (TAC) (Figure 4a), pluronic (Figure 4b) and tween 80 (Figure 4c) constituents are synthetized and therefore have well defined structural information. Ketoconazole molecule contains two chiral centers, so it forms four enantiomers. The therapeutically used ketoconazole (KET) is a racemic mixture consisting of two *cis*, (2R, 4S) - (+) KET and (2S, 4R) - (-) KET enantiomers (Novotná, et al., 2014). Considering the frequent use of ketoconazole, its chiral structure and numerous drug interactions, it is important to study the enantiospecific interactions, mainly because individual drug enantiomers may exhibit different kinetic and dynamic behavior. Studies of antifungal activities of ketoconazole *cis* enantiomers against seven strains of *Candida spp*. (Novotná, et al., 2014) demonstrated that for five strains, the (2S, 4R) - (-) KET was about seven times more potent than (2R, 4S) - (+) KET, so it seems to be a more potent inhibitor for the tested strains. In this work the enantiomer chosen to be representative of ketoconazole in NLC was (2S, 4R) - (-) KET (Figure 4d). All seven structures were optimized with DFT method using B3LYP 6-31G (d, p) basis set in the Gaussian program.

Figure 3. Snapshot representative for (a) SOS (b) SOO (c) Carnauba wax obtained after optimization.

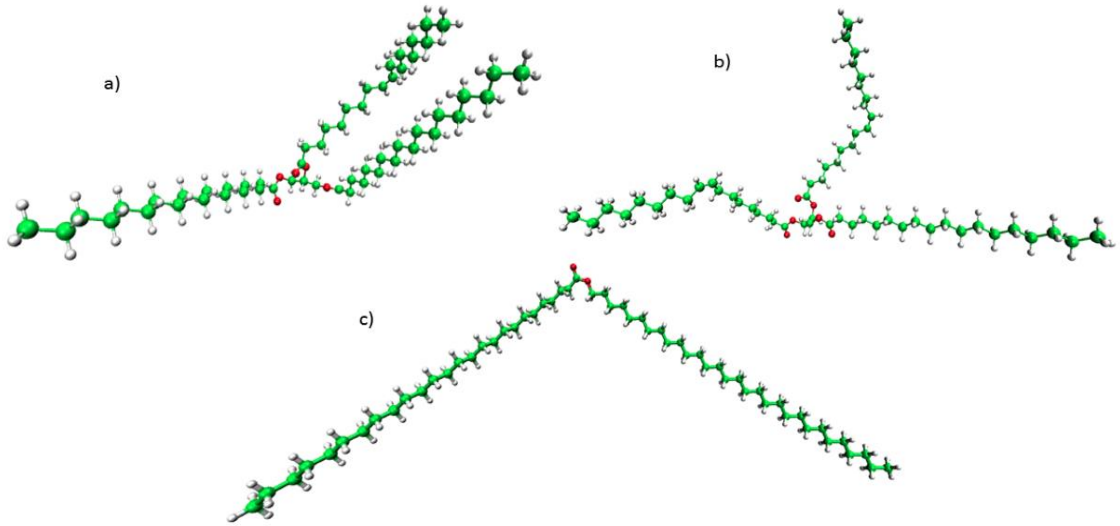

Source: Authors.

Figure 4. Snapshot representative for (a) TAC (b) Pluronic (c) tween 80 (d) ketoconazole obtained after optimization.

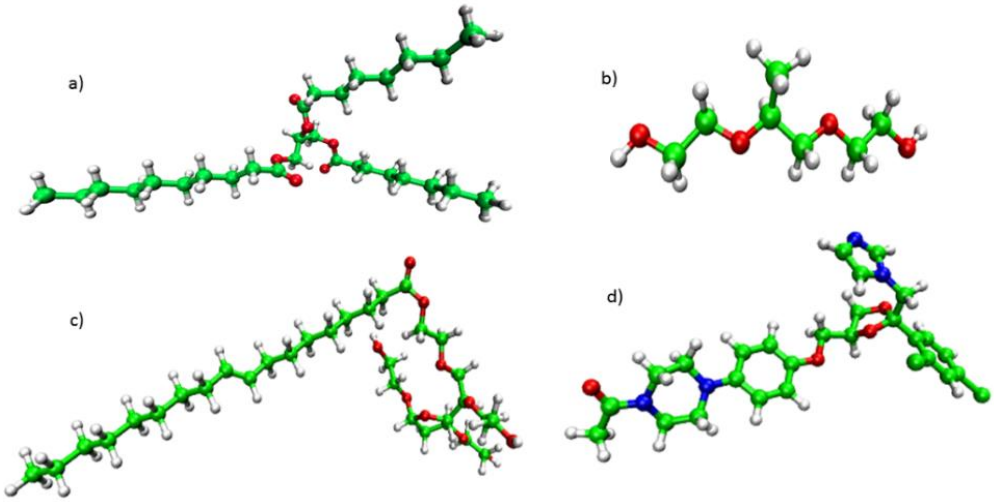

Source: Authors.

Figures 3 and 4 shows the representative snapshot of the SOS, SOO, Carnauba Wax, TAC, Pluronic, tween 80 and Ketoconazole obtained after optimization molecules. Note that after stabilization, each component had a conformation of greater stability, in which are arranged the atoms of carbon (in green), hydrogen (in white), oxygen (in red) and nitrogen (in blue).

3.3 Molecular Electrostatic Potential (mep)

MEP surfaces were calculated to understand groups with the highest affinity for intermolecular interactions established between NLC constituents and ketoconazole. Figure 5 and Figure 6 show MEP surfaces generated for each structure demonstrate nucleophilic regions (negative electrostatic potential) and electrophilic regions (positive electrostatic potential). In all structures, positive electrostatic potentials were observed around hydrogen atoms, which are more susceptible to nucleophilic attack (Figure 5 and Figure 6). SOS and SOO (Figure 5a and Figure 5b, respectively) showed regions with negative electrostatic potential around oxygen atoms of acyl groups, more intensely in carbonyl portion, due to electron withdrawing effect of the carbonyl group and in unsaturated bond. In wax and TAC (Figure 5c and Figure 6a, respectively), negative potentials are observed around oxygen atoms of the acyl groups. In Tween 80 (Figure 6c), negative potential regions are observed around oxygen atoms of the acyl groups and in unsaturated bond. In Pluronic (Figure 6b) regions of negative potential are observed around oxygen atoms, the most electronegative atom of the structure. In ketoconazole (Figure 6d), negative potencials around nitrogen atom of the azole ring, oxygen atom of the carbonyl and aromatic ring. Nucleophilic regions, rich in electrons, generate negative potential and are more susceptible to electrophiles attack.

Figure 5. Snapshot representative the Molecular Electrostatic Potential (MEP) surfaces for (a) SOS (b) SOO (c) Carnauba wax. The increase of negative charges goes from the blue (positive) to red (negative).

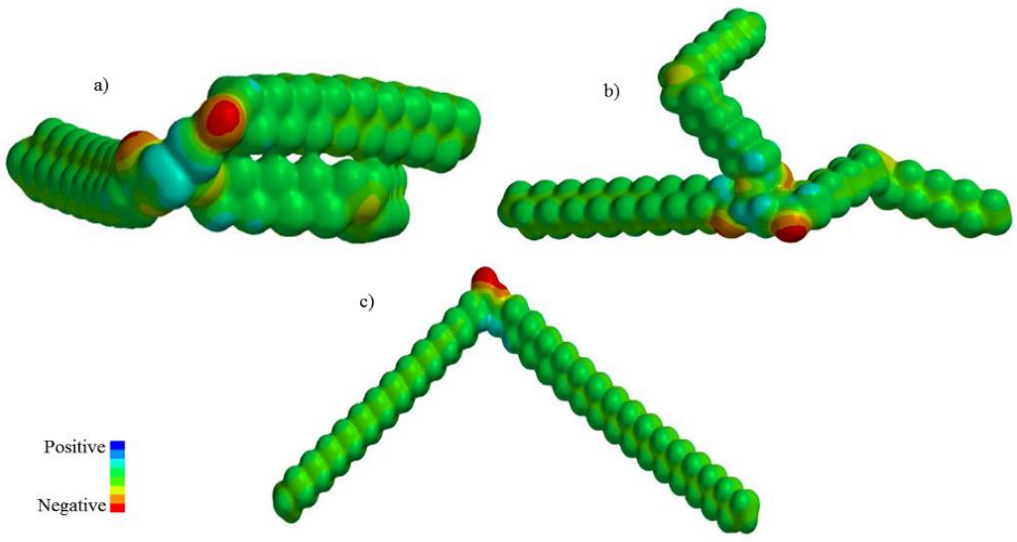

Source: Authors.

Figure 6. Snapshot representative the Molecular Electrostatic Potential (MEP) surfaces for (a) TAC (b) Pluronic (c) Tween 80 (d) Ketoconazole. The increase of negative charges goes from the blue (positive) to red (negative).

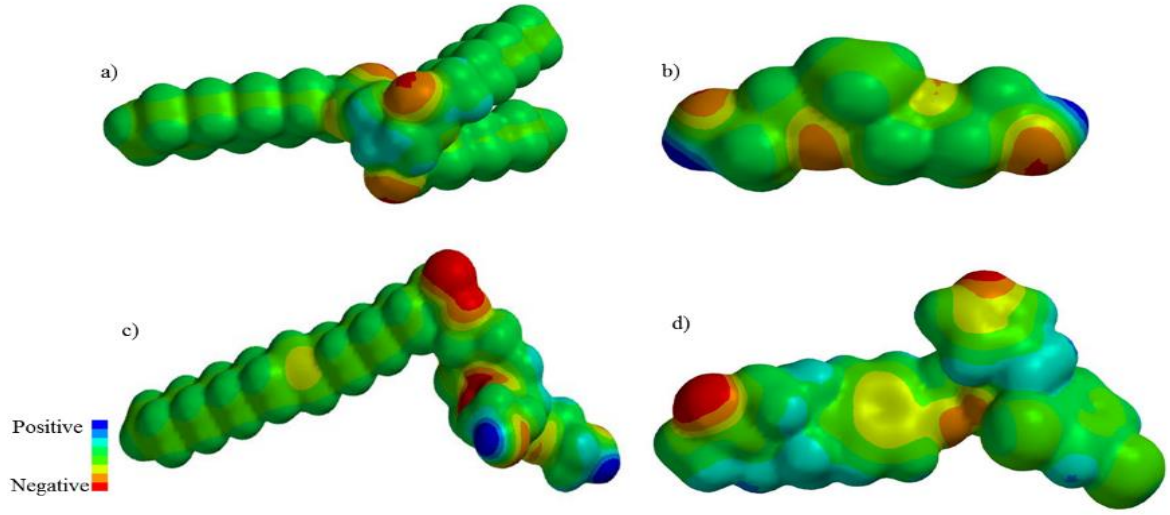

Source: Authors.

Figures 5 and 6 shows the MEP surfaces for SOS, SOO, Carnauba wax, TAC, Pluronic, tween 80 and ketoconazole. Note color spectrum from red to blue indicates the trend in relation to charge, the increase of negative charges goes from the blue (positive) to red (negative).

3.4 Electronic properties (homo and lumo)

The highest occupied molecular orbital (HOMO) and the lowest unoccupied molecular orbital (LUMO) are border orbitals and are related to the energy that the molecular orbital occupies (Namba, et al., 2008)**.** They provide information about the electron/donor or electron/acceptor character of an atom and a complex formed by charge transfer. HOMO energy is related to the ability to donate electrons, so the higher the HOMO energy, the greater the ability to donate electrons. LUMO energy is related to the ability to receive electrons from a molecule, the lower the LUMO energy, the lower the resistance to accepting electrons (Arroio, et al., 2010).

In the Table 4 the values are described the optmization energy (Hatree) of HOMO energy, LUMO energy and Gap values.

Table 4. Orbitals HOMO, LUMO and interval Gap (H-L).

Components	HOMO (Ha)*	LUMO (Ha)*	Gap (H-L)
SOS	-0,2321	-0,0583	0,1738
SOO	-0,1790	-0,0218	0,1572
Carnauba Wax	-0,2552	0,0144	0,2696
TAC	-0,2662	0,0037	0,2699
Tween 80	-0,2339	0,0211	0,255
Pluronic	-0,2522	0,0616	0,3138
Ketoconazole	-0,1821	-0,0369	0,1452

*Ha – Optmization energy (Hatree). Source: Authors.

Observed in Table 4, SOO and ketoconazole have higher HOMO energy values; therefore they have highly electron donating atoms. SOS and ketoconazole presented lower values of LUMO energy, so it can be inferred that they have acceptor atoms with less resistance to accept electrons. The Gap (H-L) range is obtained by the modulus of the difference between HOMO and LUMO energies and is an indicator of compounds reactivity. Molecules with lower Gap values (H-L) are more reactive and have lower stability (Zhang & Musgrave, 2007). According to Table 4 it can be observed ketoconazole, SOO and SOS had lower module values, so they prove to be the most reactive compounds.

3.5 Model of lipid matrix

The three-dimensional model of mixture M03 (Figure 7) was generated using Packmol program and snapshot generated in VMD. Packmol creates an optimized model for further molecular docking studies and molecular dynamics simulations. The generated model aims to ensure that short-range repulsive interactions do not disturb or interfere with simulations.

Figure 7. Snapshot representative the mixture M03. In yellow is the TAC, in pink the SOS, in green is SOO and grey is Carnauba wax.

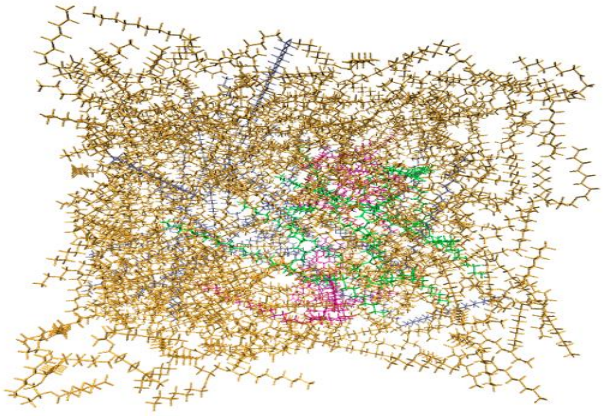

Source: Authors.

The Figure 7 is a three-dimensional representation of the M03 mixture. For the construction of this optimized model, was used the number of molecules required for each component of the M03 mixture. Note that in this mixture, the yellow molecules represent TAC, in pink the SOS, in green is SOO and gray is Carnauba Wax.

Analysis of Figure 7 shows that the model for the proposed mixture was quite satisfactory, since there was no shock between components of the mixtures, molecules were well distributed in the box space, and it was possible to create appropriate initial configurations. This molecular arrangement is fundamental to generate suitable systems for subsequent computational simulations, since it minimizes the possibility of destabilization of the system because of great repulsive interactions, which is one of the reasons for failure of more complex simulations such as molecular dynamics.

3.6 Molecular docking

Result obtained from Packmol software was used as a starting point to determine the best conformation and preferred site of ketoconazole in the selected mixture (M03). The model generated twenty iteractions, among which the one that presented the best conformation (model 10) had the lowest affinity energy, -5.3 Kcal/mol, best spatial conformation and greatest stability. The Figure 8 shows the main interactions established between ketoconazole and the other lipid matrix compounds.

Figure 8. The result of docking conformation obtained for ketoconazole.

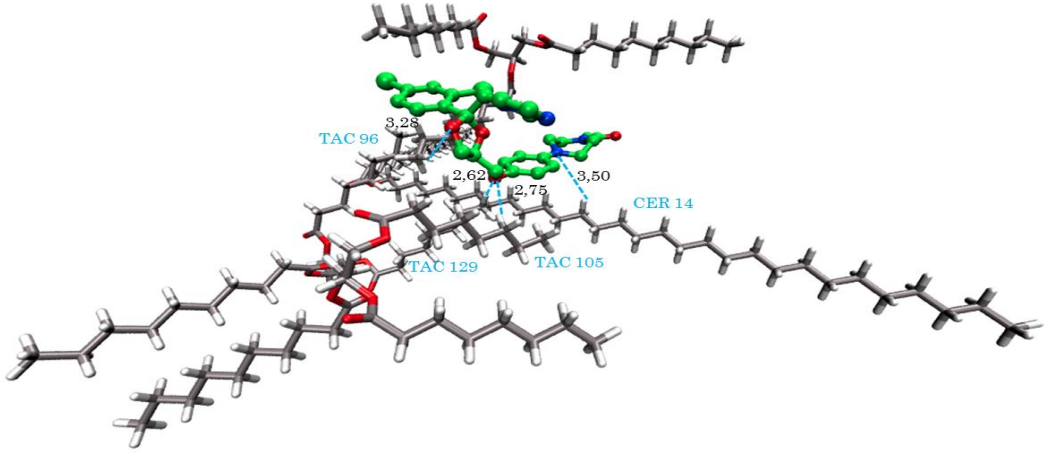

Source: Authors.

The Figure 8 is a three-dimensional representation of the molecular docking obtained between Ketoconazole and some components of the lipid matrix. Note that the Ketoconazole molecule is located in the center of Figure 8, and it is surrounded by other molecules forming several hydrogen bonds.

Hydrogen bonds mainly between ketoconazole and TAC were noted (Figure 8**).** No significant interactions were observed between ketoconazole, SOS and SOO. A hydrogen bond between the O-benzene (oxygen bound to the aromatic ring) of ketoconazole and the alkyl of TAC (H-TAC129) with bonding distance of 2.62 Å was observed. Another interaction between the same O-benzene group of ketoconazole and TAC alkyl hydrogen atom (H-TAC105) at 2.75Å was also observed. The O-alkyl group of ketoconazole established hydrogen bonding with TAC Hydrogen atom (H-TAC96) at 3.28Å. The N-benzene amino group (nitrogen attached to the aromatic ring) of ketoconazole interacted with the hydrogen atom of the wax (H-CER14) establishing hydrogen bonding with bonding distance of 3.50Å.

3.7 Molecular dynamics simulation

Initially a NLC three-dimensional model was generated with Gromacs software, using 120Å orthorhombic box and the following components: SOS, SOO, wax, TAC, Tween 80, pluronic, ketoconazole and water. After 20ns of molecular dynamics (MD) it was observed, in the Figure 9**,** that the formed system stabilized in such a way that structures agglomerated, tending to a spherical shape**,** similar to droplets of oily phase when dispersed in aqueous

phase, stabilized by surfactants, in emulsions of lipid nanoparticles (Bruxel et al., 2012). Total energy of the system was -1895.47 KJ/mol, density 0.9765 kg/m^3 and 100nm of diameter medium. Total energy remained stable during simulation.

Figure 9. The model three-dimensional (3D) of the NLC after dynamics simulation. The solvated (a) and unsolvated (b).

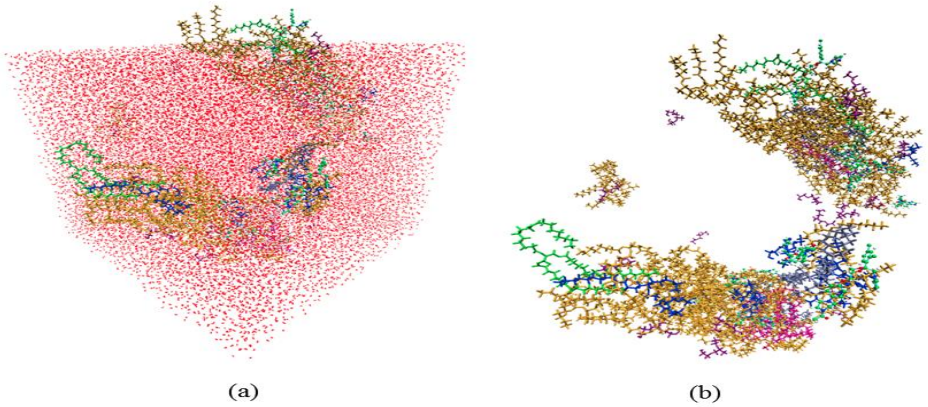

Source: Authors.

The Figure 9 is a three-dimensional representation of the NLC obtained after 20 ns of MD Simulation. On the left there is a system in a solvated system and on the right an unsolvated system (without water molecules). Note in this figure, that the molecules of the NLC components are arranged in an agglomerated form, in which we highlight the molecules of the TAC (in yellow), SOS (in pink), SOO (in green), Carnauba Wax (in gray), Ketoconazole (in green), Pluronic (in blue) and Tween 80 (in violet).

After MD simulations, hydrogen bond type interactions with ketoconazole were observed. Many biological processes are directly related to solubility of substances, which, by turn, are related to bond formation, therefore hydrogen bonds are some of the most relevant (Martins, et al., 2013). Hydrogen bonds with distances between 2.2-2.5Å are considered strong, those of 2.5-3.2Å are moderate and 3.2-4.0Å are considered weak. Hydrogen bonds are among the interactions responsible for the crystalline ordering of a system, the attraction forces that bind atoms in a crystalline lattice are directly proportional to the crystalline order, which means that the stronger the bonds, the more cohesive are the atoms of the lattice and the higher the crystal order (Klein & Dutrow, 2009), which could influence encapsulation, permeability, release and diffusion of the drug in lipid nanoparticles (Desai, et al., 2012; Wang et al., 2013). Hydrogen bonds found in this study were of moderate relative strength.

In the Table 5 shows the main interactions that occurred between ketoconazole and other NLC components with their respective binding distances, obtained after dynamics simulation.

Table 5. Main interactions between ketoconazole and other NLC components after molecular dynamics.

Interaction	Distance (Å)	Interaction	Distance (Å)
SOO 5 (O) : (H) CET 125	2,82	TAC 117 (H) : (O) CET 128	2,82
TAC 61 (H) : (O) CET 130	2,57	TAC 51 (O) : (H) CET 123	2,69
TAC 88 (O) : (H) CET 131	2,74	TAC 76 (H) : (O) CET 129	2,95
TAC 117 (O) : (H) CET 128	2,96	TAC 116 (H) : (N) CET 129	2,45

SOO and SOS: Cupuassu fat triacylglycerols / TAC: Capric/Caprylic acid triacylglycerols. Source: Authors.

Between SOO and ketoconazole the following interactions: hydrogen bonds between oxygen of SOO acyl group (SOO5) and hydrogen atom of methyl group of ketoconazole (CET125) at 2.82Å. Yet with TAC, several interactions were observed with ketoconazole molecules, a hydrogen bond between the hydrogen atom of TAC alkyl group (TAC61) and O-alkyl atom of ketoconazole (CET130) at 2.57Å. Another hydrogen bond was established between the O-acyl atom of TAC (TAC88) and H-alkyl atom of ketoconazole (CET131) at 2.74Å. Two hydrogen bonding interactions were observed among other molecules of ketoconazole (CET128) and TAC (TAC117), the first between the oxygen atom of TAC117 acyl group and CET128 H-alkyl atom at 2.96Å, and the second between TAC H-alkyl atom (TAC117) and O-benzene (oxygen bound benzene) atom of ketoconazole (CET128) at 2.82Å. Other hydrogen bonds were also observed between the O-acyl atom of TAC (TAC51) and the H-alkyl atom of ketoconazole (CET 123) at 2.69Å. The N-alkyl group of the imidazole ring of ketoconazole (CET129) interacts with the hydrogen atom of the alkyl group of TAC (TAC 116) with a value of 2.45Å. Another molecule of ketoconazole (CET129) also established hydrogen bonds with TAC, one with 2.45Å distance between the N-alkyl of the imidazole ring of ketoconazole (CET129) and H-alkyl of TAC atom (TAC116) and another with bond distance of 2.95Å between the carbonyl oxygen of the ketoconazole acyl group (CET 129) and H-alkyl of TAC (TAC 76).

3.8 Radial distribution function (RDF)

Radial distribution function represents the probability of finding an atom or molecule in a spherical shell at some distance away (r) from an atom or reference molecule. RDF, g(r), provides an estimate of spatial conformation of atoms and / or molecules relative to a focal point and demonstrates a long-range arrangement in the structure or system (Razmimanesh, et al., 2015). The figure 10 shows the estimates RDF the molecules of NLC simulated.

In the figure 10 shows RDF diagrams generated by the interaction of NLC proposed, contained Ketoconazole (CET), SOS (SOS), SOO (SOO), carnauba wax (CER), TAC (TAC), Pluronic (PLU) and Tween 80 (T80), in an unsolvated system and solvated system with water molecules (SOL).

Note that Figure 10a demonstrates RDF diagram using ketoconazole as reference molecule and related to SOS (SOS), SOO (SOO), wax (CER), TAC (TAC) and Tween 80 (T80) in a water free molecular system, calculated with a distance of up to 3.5Å from the reference molecule. No interactions with Pluronic were observed. Around 2Å a well defined and discrete peak with wax was observed, registering its first interaction in the shortest distance. This event is followed by well defined and discrete peaks around 2 Å to 2.5Å of interaction with Tween 80, SOO, SOS and TAC. RDF profile of ketoconazole showed that interactions with higher intensity peaks occurred with Tween 80 molecules suggesting its higher lipophilic affinity. Interactions were generally observed from approximately 2.0Å on.

Figure 10. RDF diagrams of the ketoconazole (CET) with the other components of the NLC in unsolvated system and solvated system with water (SOL).

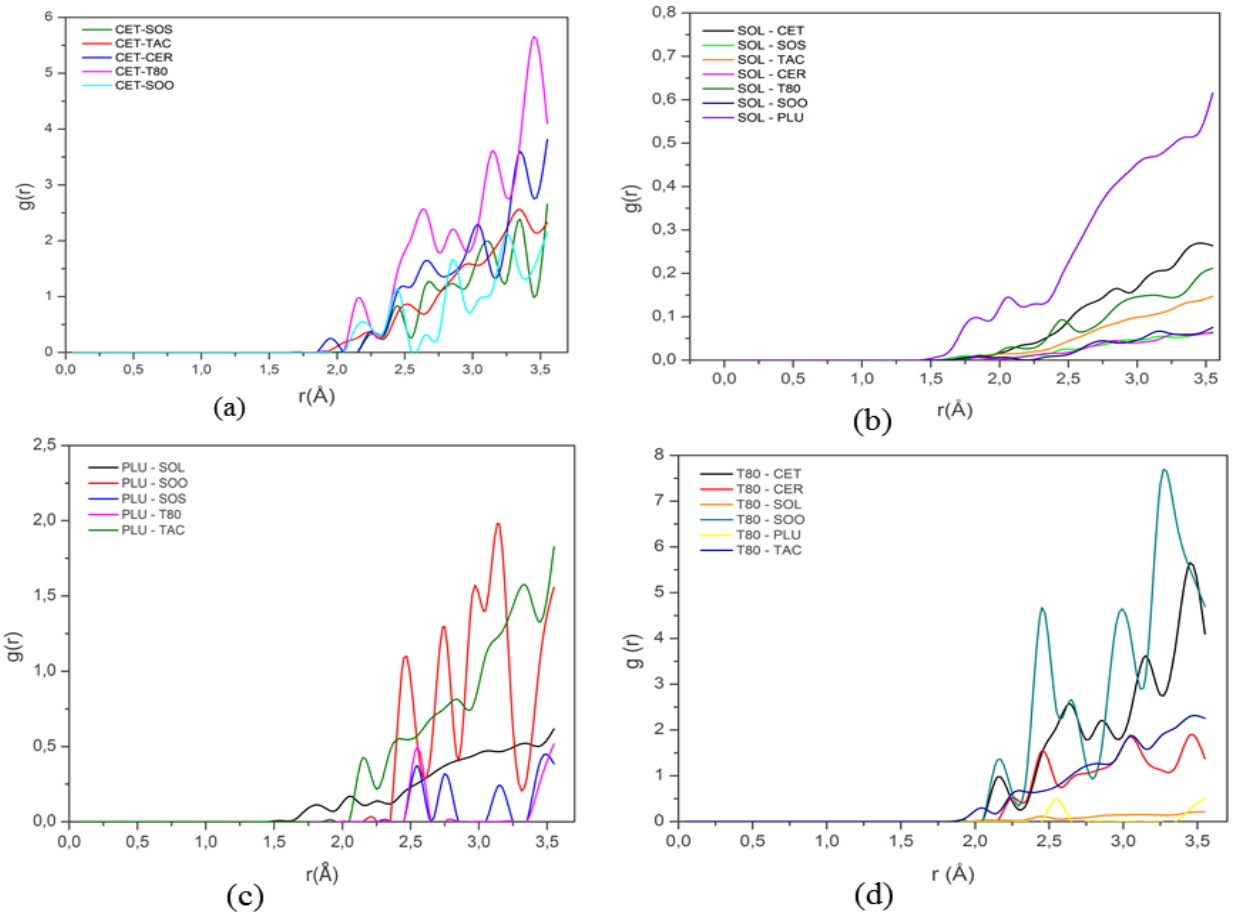

Source: Authors.

Figure 10b shows RDF diagram where water (SOL) is the reference molecule in relation to ketoconazole (CET), SOS (SOS), SOO (SOO), wax (CER), TAC (TAC), Tween 80 (T80) and Pluronic (PLU), calculated with a distance of up to 3.5Å. Well defined and discrete peaks were observed at a distance around 2.0Å in relation to Pluronic and 2.5Å in relation to Tween 80. It was observed that curves of greater intensity were obtained by interaction with Pluronic, which may suggest molecules with a more hydrophilic character at this distance. Since in aqueous environments, where water is used as a reference, the higher peaks suggest a higher hydrophilic character and the lower ones suggest a greater amount of hydrophobic regions (Wang, et al., 2013).

Figure 10c shows RDF diagram with Pluronic (PLU) as reference molecule in relation to SOS, SOO, TAC, Tween 80 (T80) and water (SOL), calculated with distance up to 3.5Å. No interactions were obtained with wax and ketoconazole. A discrete peak with water was

observed at around 1.75Å, followed by a well defined peak of medium intensity with TAC around 2.25Å, and around 2,5Å other well-defined high intensity peaks with SOO and medium intensity with Tween 80 and SOS. In general, interactions of greater intensity occurred in relation to SOO, suggesting greater affinity of its molecules to Pluronic.

Figure 10d demonstrates RDF diagram in which Tween 80 (T80) is the reference molecule related to ketoconazole (CET), wax, (CER), SOO (SOO), TAC (TAC), pluronic (PLU) and water (SOL). The first well-defined and low-intensity peak was observed at around 2.0 Å due to interaction with TAC; around 2.25Å the first interaction peak of medium intensity with ketoconazole and SOO was observed and in the range of 2.5Å interaction peaks of medium intensity with wax and another very discrete with Pluronic were also observed. In general, Tween 80 had stronger interactions with SOO and ketoconazole.

From the RDF's profiles obtained we can estimate the arrangement of the compounds in NLC; therefore, it is likely that the most hydrophilic molecules were distributed in the most distant regions of ketoconazole, such as Pluronic and water molecules on the surfaces. SOS, SOO, TAC and Tween 80 molecules were distributed in the intermediate region. Most lipophilic compounds (intermediate region molecules and wax) remained in the region closest to the drug, and the internal region of NLC.

5. Conclusion

In conclusion, we report a three-dimensional model of lipid mixture whose molecules remained well distributed and no destabilization was possible. The NLC system proposed in this work is stable and with interactions of moderate relative strength, and possibly would have little influence on the active principle diffusion. A satisfactory model of NLC containing ketoconazole was generated from Molecular Docking and Molecular Dynamics studies.

The future perspectives of this study include use this model of NLC for more computational studies of the next stages of lipophilic drug delivery system, as the evaluation of the drug release and absorption profile. As well as, make this an experimental model for the rational planning for development of lipid formulations.

References

Arroio, A., Honório, K. M., & Silva, A. B. F. da. (2010). Quantum chemical properties used in structure-activity relationship studies. *Química Nova*, *33*(3), 694–699. Doi: 10.1590/S0100-40422010000300037

Brancolini, G., Kokh, D. B., Calzolai, L., Wade, R. C., & Corni, S. (2012). Docking of Ubiquitin to Gold Nanoparticles. *ACS Nano*, *6*(11), 9863–9878. Doi:10.1021/nn303444b

Bruxel, F., Laux, M., Wild, L. B., Fraga, M., Koester, L. S., & Teixeira, H. F. (2012). Nanoemulsões como sistemas de liberação parenteral de fármacos. *Química Nova*, *35*(9), 1827–1840. Doi:10.1590/S0100-40422012000900023

Carvalho, I., Pupo, M. T., Borges, Á. D. L., & Bernardes, L. S. C. (2003). Introdução a modelagem molecular de fármacos no curso experimental de química farmacêutica. *Química Nova*, *26*(3), 428–438. Doi:10.1590/S0100-40422003000300023

Costa, R. S. da, Santos, O. V. dos, Lannes, S. C. da S., Casazza, A. A., Aliakbarian, B., Perego, P., Ribeiro-Costa, R. M., Converti, A., & Silva Júnior, J. O. C. (2020). Bioactive compounds and value-added applications of cupuassu (Theobroma grandiflorum Schum.) agroindustrial by-product. *Food Science and Technology*, *40*(2), 401–407. Doi:10.1590/fst.01119

Desai, P. V., Raub, T. J., & Blanco, M.-J. (2012). How hydrogen bonds impact P-glycoprotein transport and permeability. *Bioorganic & Medicinal Chemistry Letters*, *22*(21), 6540–6548. Doi: 10.1016/j.bmcl.2012.08.059

Engel, T., & Reid, P. (2006). *Quantum Chemistry and Spectroscopy with Spartan Student Physical Chemistry Software*. Washington: Prentice Hall.

Galindo, M.V., Paglione, I. dos S., Coelho, A. R., Leimann, F. V., & Shirai, M. A. (2020). Production of chitosan nanoparticles and application as coating in starch and poly(lactic acid) sheets. *Research, Society and Developmen*t, 9(9), 1-15. Doi:10.33448/rsd-v9i9.7694

Gilabert-Escrivá, M. V., Gonçalves, L. A. G., Silva, C. R. S., & Figueira, A. (2002). Fatty acid and triacylglycerol composition and thermal behaviour of fats from seeds of Brazilian Amazonian Theobroma species. *Journal of the Science of Food and Agriculture*, *82*(13), 1425–1431. Doi: 10.1002/jsfa.1107

Haider, M., Abdin, S. M., Kamal, L., & Orive, G. (2020). Nanostructured Lipid Carriers for Delivery of Chemotherapeutics: A Review. *Pharmaceutics*, *12*(3). Doi:10.3390/pharmaceutics12030288

Jämbeck, J. P. M., Eriksson, E. S. E., Laaksonen, A., Lyubartsev, A. P., & Eriksson, L. A. (2014). Molecular Dynamics Studies of Liposomes as Carriers for Photosensitizing Drugs: Development, Validation, and Simulations with a Coarse-Grained Model. *Journal of Chemical Theory and Computation*, *10*(1), 5–13. Doi:10.1021/ct400466m

Klein, C., & Dutrow, B. (2009). *Manual de Ciência dos Minerais*. Porto Alegre: Bookman Editora.

Lacatusu, I., Niculae, G., Badea, N., Stan, R., Popa, O., Oprea, O., & Meghea, A. (2014). Design of soft lipid nanocarriers based on bioactive vegetable oils with multiple health benefits. *Chemical Engineering Journal*, *246*, 311–321. Doi:10.1016/j.cej.2014.02.041

Lai, L., & Barnard, A. S. (2015). Functionalized Nanodiamonds for Biological and Medical Applications. *Journal of Nanoscience and Nanotechnology*, *15*(2), 989–999. Doi:10.1166/jnn.2015.9735

Lee, H., & Pastor, R. W. (2011). Coarse-Grained Model for PEGylated Lipids: Effect of PEGylation on the Size and Shape of Self-Assembled Structures. *The Journal of Physical Chemistry B*, *115*(24), 7830–7837. Doi:10.1021/jp2020148

Martínez, L., Andrade, R., Birgin, E. G., & Martínez, J. M. (2009). PACKMOL: A package for building initial configurations for molecular dynamics simulations. *Journal of Computational Chemistry*, *30*(13), 2157–2164. https://Doi.org/10.1002/jcc.21224

Martins, C. R., Lopes, W. A., & Andrade, J. B. de. (2013). Organic compound solubility. *Química Nova*, *36*(8), 1248–1255. Doi:10.1590/S0100-40422013000800026

Milanovic, J., Manojlovic, V., Levic, S., Rajic, N., Nedovic, V., & Bugarski, B. (2010). Microencapsulation of flavors in carnauba wax. *Sensors (Basel, Switzerland)*, *10*(1), 901–912. Doi:10.3390/s100100901

Morris, G.M., Huey, R., Lindstrom, W., Sanner, M.F. Belew, R.K., Goodsell, D.S., & Olson, A.J. (2009). AutoDock4 and AutoDockTools4: automated docking with selective receptor flexibility, *J. Comput. Chem*. 30, 2785–2791. Doi:10.1002/jcc.21256

Namba, A. M., Silva, V. B. da, & Silva, C. H. T. P. da. (2008). Dinâmica molecular: Teoria e aplicações em planejamento de fármacos. *Eclética Química*, *33*(4), 13–23. Retrieved from https://www.scielo.br/pdf/eq/v33n4/v33n4a02.pdf

Novotná, A., Krasulová, K., Bartoňková, I., Korhoňová, M., Bachleda, P., Anzenbacher, P., & Dvořák, Z. (2014). Dual Effects of Ketoconazole cis-Enantiomers on CYP3A4 in Human Hepatocytes and HepG2 Cells. *PLoS ONE*, *9*(10). Doi:10.1371/journal.pone.0111286

Pereira, A. S., Shitsuka, D. M., Parreira, F. J, & Shitsuka, R. (2018). *Metodologia da pesquisa Científica.* Rio Grande do Sul: Universidade Federal de Santa Maria.

Plumley, J. A., & Dannenberg, J. J. (2011). A comparison of the behavior of functional/basis set combinations for hydrogen-bonding in the water dimer with emphasis on basis set superposition error. *Journal of Computational Chemistry*, *32*(8), 1519–1527. Doi:10.1002/jcc.21729

Puri, A., Loomis, K., Smith, B., Lee, J.-H., Yavlovich, A., Heldman, E., & Blumenthal, R. (2009). Lipid-Based Nanoparticles as Pharmaceutical Drug Carriers: From Concepts to Clinic. *Critical reviews in therapeutic drug carrier systems*, *26*(6), 523–580. Retrieved from https://www.ncbi.nlm.nih.gov/pmc/articles/PMC2885142/

Quast, L. B., Luccas, V., & Kieckbusch, T. G. (2011). Physical properties of pre-crystallized mixtures of cocoa butter and cupuassu fat. *Grasas y Aceites*, *62*(1), 62–67. Doi:10.3989/gya.034010

Ramezani, M., & Shamsara, J. (2016). Application of DPD in the design of polymeric nano-micelles as drug carriers. *Journal of Molecular Graphics and Modelling*, *66*, 1–8. Doi:10.1016/j.jmgm.2016.01.010

Ramezanpour, M., Leung, S. S. W., Delgado-Magnero, K. H., Bashe, B. Y. M., Thewalt, J., & Tieleman, D. P. (2016). Computational and experimental approaches for investigating nanoparticle-based drug delivery systems. *Biochimica et Biophysica Acta (BBA) - Biomembranes*, 1858, 1688–1709. Doi:10.1016/j.bbamem.2016.02.028

Razmimanesh, F., Amjad-Iranagh, S., & Modarress, H. (2015). Molecular dynamics simulation study of chitosan and gemcitabine as a drug delivery system. *Journal of Molecular Modeling*, *21*(7), 165. Doi:10.1007/s00894-015-2705-2

Rosa, R. L. da, Serbai, L., Novak, R. S., Paula, J. de F. P. de, Toledo, A. C. O., Carvalho, V. V. M. de, & Boscardin, P. M. D. (2020). Development and evaluation of organic silicon nanoparticles. *Brazilian Journal of Development*, *6*(3), 13180–13190. Doi:10.34117/bjdv6n3-255

Salvi, V. R., & Pawar, P. (2019). Nanostructured lipid carriers (NLC) system: A novel drug targeting carrier. *Journal of Drug Delivery Science and Technology*, *51*, 255–267. Doi:10.1016/j.jddst.2019.02.017

Sant'Anna, C. M. R. (2009). Métodos de Modelagem Molecular para Estudo e Planejamento de Compostos Bioativos: Uma Introduçao. *Revista Virtual de Química*, *1*(1), 49–57. Doi:10.5935/1984-6835.20090007

Santos, G. S. dos, Pereira, G. G., Bender, E. A., Colomé, L. M., Guterres, S. S., Carvalho, D. C. M. de, & Weissmüller, G. (2012). Desenvolvimento e caracterização de nanopartículas lipídicas destinadas à aplicação tópica de dapsona. *Química Nova*, *35*(7), 1388–1394. Doi:10.1590/S0100-40422012000700019

Silva, J. C., Plivelic, T. S., Herrera, M. L., Ruscheinsky, N., Kieckbusch, T. G., Luccas, V., & Torriani, I. L. (2009). Polymorphic Phases of Natural Fat from Cupuassu (Theobroma grandiflorum) Beans: A WAXS/SAXS/DSC Study. *Crystal Growth & Design*, *9*(12), 5155–5163. Doi:10.1021/cg901081j

Silva, J. D. de S., Leite, S. da C., Silva, M. T. S. da, Meirelles, L. M. A., & Andrade, A. W. L. (2020). In silico evaluation of the inhibitory effect of antiretrovirals Atazanavir and Darunavir on the main protease of SARS-CoV-2: docking studies and molecular dynamics. *Research, Society and Development*, *9*(8). Doi:10.33448/rsd-v9i8.6562

Silva, N. de F., da Silva, R. L., Almeida, K. de O., Nascimento-Júnior, A. E. S. do, Brasil, D. do S. B., Silva-Júnior, J. O. C., Teixeira, F. M., & Ribeiro-Costa, R. M. (2017). Study of molecular interactions between Chitosan and Vi Antigen. *Journal of Molecular Graphics and Modelling*, *72*, 148–155. Doi:10.1016/j.jmgm.2016.12.015

Souto, E. B., Mehnert, W., & Müller, R. H. (2006). Polymorphic behaviour of Compritol®888 ATO as bulk lipid and as SLN and NLC. *Journal of Microencapsulation*, *23*(4), 417–433. Doi:10.1080/02652040600612439

Souto, F. L. G. (2013). *Obtenção e caracterização de carreadores lipídicos nanoestruturados a partir de gordura vegetal de Cupuassu (Theobroma grandiflorum).* Belém: Universidade Federal do Pará.

Todorova, N., Chiappini, C., Mager, M., Simona, B., Patel, I. I., Stevens, M. M., & Yarovsky, I. (2014). Surface Presentation of Functional Peptides in Solution Determines Cell Internalization Efficiency of TAT Conjugated Nanoparticles. *Nano Letters*, *14*(9), 5229–5237. Doi:10.1021/nl5021848

Van Der Spoel, D., Lindahl, E., Hess, B., Groenhof, G., Mark, A. E., & Berendsen, H. J. C. (2005). GROMACS: Fast, flexible, and free. *Journal of Computational Chemistry*, *26*(16), 1701–1718. Doi:10.1002/jcc.20291

Villalobos-Hernández, J. R., & Müller-Goymann, C. C. (2006). Sun protection enhancement of titanium dioxide crystals by the use of carnauba wax nanoparticles: The synergistic interaction between organic and inorganic sunscreens at nanoscale. *International Journal of Pharmaceutics*, *322*(1–2), 161–170. Doi:10.1016/j.ijpharm.2006.05.037

Wang, X.-Y., Zhang, L., Wei, X.-H., & Wang, Q. (2013). Molecular dynamics of paclitaxel encapsulated by salicylic acid-grafted chitosan oligosaccharide aggregates. *Biomaterials*, *34*(7), 1843–1851. Doi:10.1016/j.biomaterials.2012.11.024

Yang, Y., Corona, A., Schubert, B., Reeder, R., & Henson, M. A. (2014). The effect of oil type on the aggregation stability of nanostructured lipid carriers. *Journal of Colloid and Interface Science*, *418*, 261–272. Doi:10.1016/j.jcis.2013.12.024

Xu, D., Martin, C., & Schulten, K. (1996). Molecular Dynamic Study of Early Picosecond events in the bacteriorhodopdin photocicly: Dieletric response vibrational cooling and the J, K intermediates. *Biophys. J***,** 70, 453-460. Doi:10.1016/S0006-3495(96)79588-7

Zhang, G., & Musgrave, C. B. (2007). Comparison of DFT Methods for Molecular Orbital Eigenvalue Calculations. *The Journal of Physical Chemistry A*, *111*(8), 1554–1561. Doi:10.1021/jp061633o

Zhang, S., Sun, H.-J., Hughes, A. D., Moussodia, R.-O., Bertin, A., Chen, Y., Pochan, D. J., Heiney, P. A., Klein, M. L., & Percec, V. (2014). Self-assembly of amphiphilic Janus dendrimers into uniform onion-like dendrimersomes with predictable size and number of bilayers. *Proceedings of the National Academy of Sciences of the United States of America*, *111*(25), 9058–9063. Doi:10.1073/pnas.1402858111

Percentage of contribution of each author in the manuscript

Ana Paula Bastos Ferreira Vieira – 30%

Natália de Farias Silva – 30%

Davi do Socorro Barros Brasil – 20%

José Otávio Carréra Silva Júnior – 10%

Roseane Maria Ribeiro Costa – 10%